MOLECULAR AND CELLULAR BIOLOGY, May 2009, p. 2694–2703 Vol. 29, No. 10
0270-7306/09/$08.00+0 doi:10.1128/MCB.01460-08

ADAM9 Is Involved in Pathological Retinal Neovascularization[▽]

Victor Guaiquil,[1]† Steven Swendeman,[1]† Tsunehiko Yoshida,[2] Sai Chavala,[3] Peter A. Campochiaro,[2] and Carl P. Blobel[1,4]*

Arthritis and Tissue Degeneration Program, Hospital for Special Surgery, New York, New York 10021[1]; Wilmer Eye Institute, Johns Hopkins University School of Medicine, Baltimore, Maryland 21287[2]; Department of Ophthalmology, Duke University Medical Center, P.O. Box 3802, Durham, North Carolina 27710[3]; and Departments of Medicine and Physiology, Biophysics, and Systems Biology, Weill Medical College of Cornell University, New York, New York 10021[4]

Received 17 September 2008/Returned for modification 20 October 2008/Accepted 26 February 2009

Pathological ocular neovascularization, caused by diabetic retinopathy, age-related macular degeneration, or retinopathy of prematurity, is a leading cause of blindness, yet much remains to be learned about its underlying causes. Here we used oxygen-induced retinopathy (OIR) and laser-induced choroidal neovascularization (CNV) to assess the contribution of the metalloprotease-disintegrin ADAM9 to ocular neovascularization in mice. Pathological neovascularization in both the OIR and CNV models was significantly reduced in *Adam9*$^{-/-}$ mice compared to wild-type controls. In addition, the level of ADAM9 expression was strongly increased in endothelial cells in pathological vascular tufts in the OIR model. Moreover, tumor growth from heterotopically injected B16F0 melanoma cells was reduced in *Adam9*$^{-/-}$ mice compared to controls. In cell-based assays, the overexpression of ADAM9 enhanced the ectodomain shedding of EphB4, Tie-2, Flk-1, CD40, VCAM, and VE-cadherin, so the enhanced expression of ADAM9 could potentially affect pathological neovascularization by increasing the shedding of these and other membrane proteins from endothelial cells. Finally, we provide the first evidence for the upregulation of ADAM9-dependent shedding by reactive oxygen species, which in turn are known to play a critical role in OIR. Collectively, these results suggest that ADAM9 could be an attractive target for the prevention of proliferative retinopathies, CNV, and cancer.

Ocular neovascularization is one of the leading causes of blindness in humans and is found in diverse eye diseases including diabetic retinopathy, age-related macular degeneration, and retinopathy of prematurity (3, 4, 6). In addition, pathological neovascularization also has critical roles in other diseases such as cancer and rheumatoid arthritis (12, 14). Although proteins with crucial functions in pathological neovascularization are considered to be important targets for the treatment of tumor growth (5), proliferative retinopathies (19), and rheumatoid arthritis (12), much remains to be learned about the identity of these molecules and the mechanisms underlying their function. In this study, we focused on the contribution of a disintegrin and metalloprotease, ADAM9, to pathological neovascularization.

ADAM9, one of the first ADAM proteins to be identified and characterized, is a membrane-anchored metalloproteinase containing an N-terminal prodomain followed by a metalloprotease domain, a disintegrin domain and cysteine-rich region, an epidermal growth factor (EGF) repeat, a transmembrane domain, and a cytoplasmic tail with potential SH3 ligand domains (25). ADAM9 is catalytically active in both biochemical and cell-based assays and can cleave several membrane proteins including EGF and FGFR2iiib when it is overexpressed together with these substrates (10, 15, 16). In addition, ADAM9 is thought to participate in cell-cell interactions by binding to integrins (13, 30). Mice lacking ADAM9 have no evident major abnormalities during development or adult life (24) but show reduced levels of tumorigenesis in a mouse model for prostate cancer (15). In the current study, we evaluated whether ADAM9 contributes to pathological neovascularization using a mouse model for retinopathy of prematurity, the oxygen-induced retinopathy (OIR) model, as well as a model of laser-induced choroidal neovascularization (CNV). Moreover, we determined how the lack of ADAM9 affects the growth of heterotopically injected tumor cells in mice. Finally, we assessed whether overexpressed ADAM9 can process substrate proteins with known roles in angiogenesis and tested whether the catalytic activity of endogenous ADAM9 is regulated by reactive oxygen species (ROS) in cell-based assays, as ROS upregulate the expression of ADAM9 (20, 22) and are known to play important roles in pathological retinal neovascularization (9, 27).

MATERIALS AND METHODS

Materials. All chemicals and reagents were purchased from Sigma unless indicated otherwise. Isolectin B4 was obtained from Vector Laboratories (Burlingame, CA), rabbit anti-mouse NG2 was obtained from Chemicon International (Temecula, CA), and rat anti-CD31 was obtained from BD Biosciences–Pharmingen (San Diego, CA). The anti-ADAM9 and -ADAM15 monoclonal antibodies for immunofluorescence and immunohistochemistry (11, 24) and the polyclonal anti-ADAM9 antibodies for Western blotting (25) were previously described.

Western blot analysis. Western blots of ADAM9 expression in the mouse retina were performed as follows. Mice were sacrificed by CO_2 inhalation according to guidelines of the American Veterinary Association, and their intact eyes were removed, washed once in phosphate-buffered saline (PBS), and dissected to isolate the retinae. These were immersed in ice-cold cell lysis buffer (PBS, 1% NP-40, protease inhibitor cocktail) (2) in a 1.5-ml tube, disrupted using a small Teflon pestle (Lake Charles Manufacturing, Lake Charles, LA), and centrifuged for 10 min at 16,000 × *g*, and the supernatants were removed and

* Corresponding author. Mailing address: Arthritis and Tissue Degeneration Program, Caspary Research Building, Rm. 426, Hospital for Special Surgery, 535 East 70th Street, New York, NY 10021. Phone: (212) 606-1429. Fax: (212) 774-2560. E-mail: blobelc@hss.edu.
† V.G. and S.S. contributed equally.
▽ Published ahead of print on 9 March 2009.

incubated with concanavalin A-Sepharose 4B beads (GE Healthcare, Piscataway, NJ) to enrich for N-linked glycoproteins. Bound material was removed by boiling in sodium dodecyl sulfate-polyacrylamide gel electrophoresis sample buffer, reduced with 50 mM dithiothreitol, and subjected to sodium dodecyl sulfate-polyacrylamide gel electrophoresis and immunoblotting as described previously (25). Western blotting of ADAM9 in immortalized mouse embryonic fibroblasts (mEFs) with anti-mouse ADAM9 cytotail antibodies and of pig aortic endothelial (PAE) cells with anti-human ADAM9 cytotail antibodies was performed as described previously (24).

Mouse model for OIR. The response of wild-type and *Adam9*$^{-/-}$ mice to relative hypoxia was assessed using the OIR model as described previously (4, 8, 11, 21). Since the animals were of mixed genetic background (129/SvJ and C57BL/6J), some experiments were performed by comparing wild-type ($n = 10$) and *Adam9*$^{-/-}$ ($n = 9$) littermates that were offspring of heterozygous *Adam9*$^{+/-}$ parents. Moreover, to increase the number of animals included in this analysis, *Adam9*$^{-/-}$ or wild-type offspring were collected from one pair of heterozygous *Adam9*$^{+/-}$ parents. The resulting wild-type or *Adam9*$^{-/-}$ mice were mated with one another to generate litters of wild-type or *Adam9*$^{-/-}$ mice that were closely related, as they were derived from the same heterozygous grandparents.

For the OIR model, mice were exposed to 75% oxygen from postnatal day 7 (P7) to P12 in a Plexiglas chamber connected to an oxygen regulator (Pro-Ox, model 110; Reming Bioinstruments, Redfield, NY) along with their nursing mother. At P12, the animals were returned to room air (21% oxygen). The resulting relative hypoxia triggers a proliferative response in the retinal vasculature (4). The mice were kept in normoxic conditions until P17 and then sacrificed. Following euthanasia, both eyes were removed and fixed in 4% paraformaldehyde (PFA). The next day, one eye was processed for sectioning, and the second eye was processed for a whole-mount analysis of neovascularization. Eyes destined for histological evaluation of neovascularization were embedded in paraffin, sectioned (6-μm thickness), and stained with hematoxylin and eosin. About 150 sections were prepared per eye, and five sections on each side of the optic nerve, 30 to 90 μm apart, were used to assess neovascularization in a double-blinded manner by counting endothelial cell nuclei on the vitreal side of the internal limiting membrane, as previously described (11). The number of endothelial nuclei per section was averaged for each eye, and the unpaired Student *t* test (equal variation, two sided) was used to determine the statistical significance of differences between *Adam9*$^{-/-}$ and wild-type mice.

The second eye from each animal was used to measure the size of the central avascular area that develops in retinae of mice subjected to the OIR model. After overnight fixation with 4% PFA, the eyes were washed five times with PBS and incubated overnight in lectin blocking buffer (LBB) (PBS, 1% bovine serum albumin, 0.1% Triton X-100, 0.1 M glycine). The retinae were then excised, flat mounted onto microscope slides, and incubated with LBB for 2 h. Fluorescein-labeled isolectin B4 diluted 1:200 in 0.2× LBB was added and incubated overnight at 4°C. The retinae were washed twice in PBS, excess fluid was absorbed with filter paper, and the retinae were then mounted in fluorescent mounting medium (Dako). The samples were photographed using a Nikon Eclipse E600 fluorescent microscope with a 2× objective and a Qimaging Retiga EXi camera. Images were processed with QCapture 2.68.04 software, keeping the exposure and gain constant for all samples. The sizes of the avascular area and the total retina were outlined using NIH ImageJ software and used to calculate the percentage of the avascular area compared to the total retina area.

Assessment of developmental retinal angiogenesis. To compare developmental retinal angiogenesis between wild-type and *Adam9*$^{-/-}$ mice, we focused on P6, as the vascular bed covers about two-thirds of the retina at that stage (7). Therefore, any significant defects in developmental retinal angiogenesis and growth of the vascular bed should be apparent in a comparison of wild-type and *Adam9*$^{-/-}$ mice at P6. Retinae were prepared for whole-mount staining with fluorescein-labeled isolectin B4 to visualize endothelial cells after removal of the hyaloid vessels and then photographed, as described above. The area of the retina covered by the developing vascular bed was outlined using NIH ImageJ software, and its size relative to that of the retina was used to determine the percentage of the total retinal area covered by retinal vasculature.

Mouse model of CNV. CNV was triggered by laser photocoagulation-induced rupture of Bruch's membrane as described previously (23). Briefly, 5- to 6-week-old male and female wild-type and *Adam9*$^{-/-}$ mice were anesthetized with ketamine hydrochloride (100 mg/kg body weight), and pupils were dilated with 1% tropicamide. Burns (75-μm spot size, 0.1-s duration, and 120 mW) were performed in the 9, 12, and 3 o'clock positions of the posterior pole of the eye with the slit-lamp delivery system of an OcuLight GL diode laser (Iridex, Mountain View, CA) using a handheld coverslip as a contact lens to view the retina. The production of a bubble at the time of laser, which indicates rupture of Bruch's membrane, is an important factor in obtaining CNV; therefore, only burns in which a bubble was produced were included in the study. After 14 days, the mice were perfused with 1 ml of PBS containing 50 mg/ml of fluorescein-labeled dextran (average molecular weight of 2×10^6; Sigma), and choroidal flat mounts were examined by fluorescence microscopy. Images were captured with a Nikon DXM1200 digital still camera. Image analysis software (Image-Pro Plus; Media Cybernetics, Silver Spring, MD) was used to measure the total area of CNV at each rupture site, with the investigator masked with respect to treatment group.

Immunohistochemistry and immunofluorescence analysis. Frozen and paraffin-embedded samples were used for immunostaining studies. Eyes and tumors were fixed in fresh 4% PFA overnight at 4°C, washed three times with PBS, and then stored in 70% ethanol or processed for paraffin embedding. For frozen sections, PBS-washed samples were immersed in 20% sucrose overnight at 4°C and then frozen in Tissue-Tek OCT compound (Sakura Finetek, Torrance, CA) mixed with 20% sucrose in a 1:1 ratio. Sections (10 μm) were cut, mounted onto slides, and postfixed with ice-cold acetone for 10 min. Both frozen and paraffin sections were immersed in 0.3% and 3% H_2O_2, respectively, to inactivate the endogenous peroxidase, preincubated with 10% normal goat serum–2% bovine serum albumin–PBS for 1 h, and then incubated for 1 h with anti-ADAM9 m9-2 monoclonal antibodies (24) or anti-ADAM15 or anti-platelet endothelial cell adhesion molecule 1 (PECAM-1/CD31) antibodies (11). Bound antibodies were detected with biotin-conjugated anti-mouse or anti-rabbit immunoglobulin G followed by horseradish peroxidase-avidin (Vector Labs). After development with diaminobenzidine solution (Vector Laboratories), the sections were counterstained with hematoxylin.

Flat-mounted retinae were incubated with modified LBB (0.5% Triton X-100) for 4 h, washed three times with PBS, and incubated with anti-NG2 (pericyte marker) or anti-ADAM9 m9-2 (24) antibody overnight at 4°C. Retinae were washed three times with PBS, and secondary Texas Red anti-rabbit antibodies (Jackson Immunoresearch, West Grove, PA) or anti-mouse Alexa 488 (Molecular Probes, Eugene, OR) antibodies were added. After 2 h, retinae were washed three times with PBS and then stained overnight with isolectin-fluorescein isothiocyanate (FITC) or isolectin-tetramethylrhodamine isothiocyanate to mark endothelial cells, washed with PBS, and processed as described above.

In addition, 6-μm sections of paraffin-embedded eyes were analyzed by histochemistry and immunofluorescence. Eye sections were deparaffinized, rehydrated through a graded alcohol series, and heated in 10 mM sodium citrate for antigen retrieval. Samples were treated as described above for biotin/avidin staining or Alexa 488-conjugated secondary antibodies against the primary anti-ADAM9 m9-2 monoclonal antibody.

Heterotopic injection of B16F0 mouse melanoma cells. Age- and sex-matched litters of wild-type and *Adam9*$^{-/-}$ mice, derived from *Adam9*$^{+/-}$ grandparents as described above, were injected subcutaneously with 1×10^6 B16F0 mouse melanoma cells. All animals in a given experiment were sacrificed at the same time, between 2 and 3 weeks after injection depending on the tumor burden in animals with the fastest tumor growth, and the tumors were removed and weighed. For quantitation and comparison of individual trials, the average weight of tumors from wild-type controls in a given experiment was used as a reference to calculate the weight of each tumor as a percentage of the wild-type average. The unpaired Student *t* test was used for statistical evaluation. Immunofluorescence was performed to evaluate the vascularity of the tumor specimens in frozen sections incubated with anti-PECAM/CD31 as described above. Bound antibodies were detected with Cy3-conjugated AffiniPure donkey anti-rat immunoglobulin G (Jackson Immunoresearch, West Grove, PA).

Construction of expression plasmids and cell-based protein ectodomain shedding assays. To generate expression plasmids for alkaline phosphatase (AP)-tagged receptors with known roles in angiogenesis, cDNAs for murine VE-cadherin, Tie-2, CD40, EphB4, EphrinB2, CD34, VCAM-1, ICAM-1, and E-selectin were obtained from the ATCC. The cDNA for Flk1 was a kind gift of Urban Deutsch (University of Berne, Bern, Switzerland). All AP-tagged fusion proteins were designed to include at least the first extracellular domain as well as the transmembrane domain and cytoplasmic tail of the candidate substrate. The following primers were used to generate PCR products corresponding to the carboxyl end of each open reading frame, using the full-length cDNA as a template: 5′-GATGCTCTTTGGAAACTGAATGGCAC CA-3′ and 5′-AGTCGCTGTCTTGTCAATTCCAAAAGCGT-3 (amino acids 605 to 859) for FLK-1, 5′-ATGACGTATGATGAAGCCAGTGCA-3′ and 5′-GTTCCTGATTGTTTTGAACCTAGA-3′ (amino acids 31 to 612) for E-selectin, 5′-ATGAGTCTTGACAACAACGGTA-3′ and 5′-TCACAATTC GGTATCAGCCACCACG-3′ (amino acids 31 to 385) for CD34, 5′-ACTG CATGCAGAGAAAAACAGTA-3′ and 5′-TCACTGTCTCTCCTGCACTG A-3′ (amino acids 24 to 278) for CD40, 5′-AATGCCCAGACATC TGTGT CCCCC-3′ and 5′-TCAGGGAGGCGTGGCTTGTG-3′ (amino acids 26 to

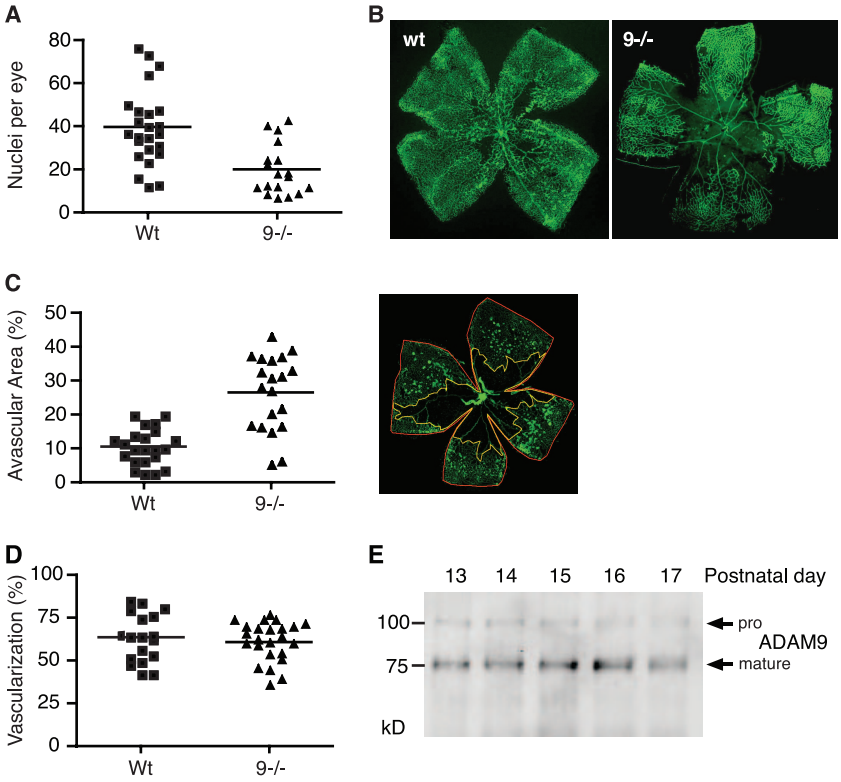

FIG. 1. Reduced oxygen-induced retinopathy in *Adam9*$^{-/-}$ mice compared to controls. (A) *Adam9*$^{-/-}$ mice and wild-type controls were subjected to the OIR model (see Materials and Methods for details). Sections of their retinae were then used to determine the number of neovascular nuclei on the vitreous side of the internal limiting membrane (see Materials and Methods for details). Each point represents the average number of nuclei per section of one animal. The results demonstrate reduced proliferative retinopathy in the absence of ADAM9 (n = 24 for wild-type [Wt] mice, and n = 18 for *Adam9*$^{-/-}$ [9−/−] mice; $P < 0.0001$). (B) Whole-mount analysis of a retina of an *Adam9*$^{-/-}$ mouse and a wild-type control subjected to the OIR model (for each genotype, one representative FITC-isolectin-stained example of over 15 analyzed retinae is shown). The central avascular area is increased in the *Adam9*$^{-/-}$ retina compared to that of the wild-type control. (C) Quantitation of the avascular area in relationship to the total size of the retina corroborates the increased avascular area in *Adam9*$^{-/-}$ mice ($P < 0.0001$). An example of how the size of the avascular area was determined using NIH Image software is shown at the right (see Materials and Methods for details). (D) Analysis of retinal developmental angiogenesis at P6. Retinae of 6-day-old wild-type and *Adam9*$^{-/-}$ mice were stained with FITC-isolectin to visualize the vascular bed, and the ratio of the surface area covered by the vascular tree was calculated as a percentage of the surface area of the whole retina. No significant difference in the development of the vascular bed between *Adam9*$^{-/-}$ mice and wild-type controls was observed. (E) Western blots of extracts of one retina per lane taken from wild-type mice between 1 and 5 days after ending their exposure to high oxygen (corresponds to P13 to P17, as indicated on the blot). The blots were probed with anti-ADAM9 cytoplasmic-domain antibodies and show slightly increased levels of mature ADAM9 on days 15 and 16 compared to the other days.

532) for ICAM-1, 5′-GAGATCTCCCCTGAATACA-3′ and 5′-CTACACTT TGGATTTCTGTGC-3′ (amino acids 28 to 739) for VCAM-1, and 5′-TCC CTGCAAACAACAAGTGATCA-3′ and 5′-AAAGTTGCCCTCTCCGATC ACG-3′ (amino acids 580 to 833) for Tie-2.

Each amplified cDNA was cloned in frame with human AP into pAP-tag−5 (Genehunter, Nashville, TN), and all constructs were sequenced to rule out undesired mutations.

Stimulation of ADAM9-dependent shedding by ROS. Expression constructs for ADAM9 and the catalytically inactive ADAM9E>A mutant were described previously (16). AP shedding assays were performed as described previously (17, 18, 24) using mEF cells and PAE cells (kindly provided by Shahin Rafii). ROS assays were performed using a modified version of the procedure reported previously by Sung et al. (22). Specifically, 20 h posttransfection, cells maintained at 50 to 60% density were washed twice with OptiMem for 1 h and then cultured in OptiMem with various concentrations of H_2O_2 for 5 h. The supernatants and lysates were assayed in triplicate for AP activity (17, 18, 29). All data are representative of at least three independent experiments.

RESULTS

Reduced oxygen-induced retinopathy in *Adam9*$^{-/-}$ mice. To address a potential role of ADAM9 in pathological retinal neovascularization, we subjected *Adam9*$^{-/-}$ mice and wild-type controls to a mouse model of OIR (see Materials and Methods for details). As shown in Fig. 1A, the number of vascular cell nuclei that contributed to pathological neovascularization in *Adam9*$^{-/-}$ mice was significantly reduced compared to that of highly related litters of wild-type controls (n = 24 [average of 39.7 and standard error of the mean {SEM} of 3.6] for wild-type mice versus n = 18 [average of 19.9 and SEM of 2.8] for knockout mice; $P < 0.0001$). When *Adam9*$^{-/-}$ and wild-type littermates obtained from heterozygous *Adam9*$^{+/-}$ parents (see Materials and Methods for details) were subjected to the OIR model, the results corroborated a significant reduction of pathological neovascularization in *Adam9*$^{-/-}$ mice compared to that of wild-type controls (n = 10 [average of 22.4 and SEM of 1.8] for wild-type mice versus n = 9 [average of 9.6 and SEM of 1.4] for knockout mice; $P < 0.0001$). Moreover, whole-mount preparations of retinae stained with FITC-lectin to label endothelial cells showed a larger central avascular area

and strongly reduced tuft formation in *Adam9*$^{-/-}$ retinae compared to wild-type controls (Fig. 1B). On average, the ratio of the retinal avascular area was significantly larger in *Adam9*$^{-/-}$ mice (27%; $n = 20$ [SEM = 2.4]) than in wild-type controls (10%; $n = 22$ [SEM = 1.1]; $P < 0.0001$) (Fig. 1C). When we compared the sizes of the retinal vascular bed at P6 in *Adam9*$^{-/-}$ mice and wild-type controls to determine whether ADAM9 has a role in developmental retinal angiogenesis, we found no significant difference at this stage (Fig. 1D). Taken together, these finding indicate that ADAM9 is involved in pathological neovascularization during OIR in mice but not in developmental retinal angiogenesis at P6.

To determine whether the expression of ADAM9 in the retina changes during an OIR experiment, we performed a Western blot on extracts of retinae from mice at P13 to P17, corresponding to 1 to 5 days after removal from the 75% oxygen chamber (Fig. 1E). ADAM9 protein levels were comparable in all samples, with a slight increase detected at P15 and P16. Since a Western blot of extracts of whole retinae might not uncover local changes in ADAM9 expression in a small population of cells, we also stained whole-mount preparations of retinae of wild-type mice subjected to the OIR model with a monoclonal antibody against ADAM9 (detected with an Alexa 488-labeled secondary antibody in Fig. 2A and B) and with CD31 (Cy3 labeled) to mark endothelial cells (Fig. 2A). Immunofluorescence microscopy showed high levels of expression of ADAM9 in neovascular tufts (Fig. 2A and B), in which ADAM9 expression colocalized with CD31-labeled endothelial cells (Fig. 2A) but not with NG2-labeled pericytes (Fig. 2B). There was no difference in the distribution of NG2 staining in retinal tufts of wild-type and *Adam9*$^{-/-}$ mice after OIR (data not shown). In retinae from *Adam9*$^{-/-}$ mice subjected to OIR, the anti-ADAM9 antibody did not label neovascular tufts, even though these could be clearly visualized with anti-CD31, demonstrating that the staining in wild-type retinae was specific for ADAM9 (Fig. 2A and B, bottom). A comparison of the expression of ADAM9 with that of the pericyte marker NG2 showed little, if any, overlap in neovascular tufts in wild-type retinae (Fig. 2B), suggesting that ADAM9 is not expressed in pericytes. The high level of expression of ADAM9 in neovascular tufts was also corroborated in a horseradish peroxidase-stained section of a retina from a wild-type mouse after OIR and by immunofluorescence analysis (Fig. 2C). Sections of a tuft from an *Adam9*$^{-/-}$ mouse served as a control for the specificity of the anti-ADAM9 antibody (Fig. 2C, bottom). Finally, antibodies against ADAM15, which is also highly expressed in neovascular tufts (11), served as a positive control for these samples in that they stained the tufts of both wild-type and *Adam9*$^{-/-}$ retinae (Fig. 1C).

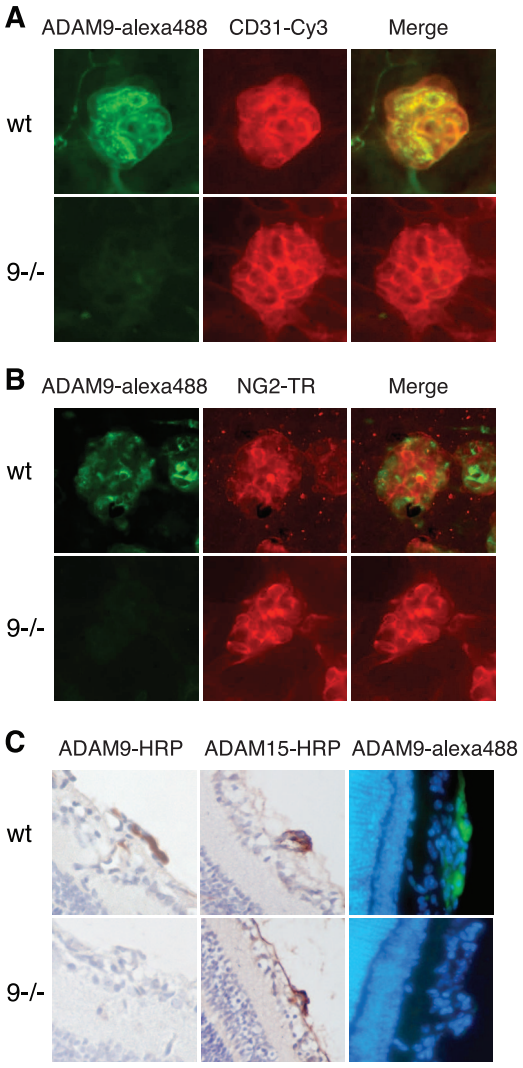

FIG. 2. Immunofluorescence and immunohistochemical analysis of the expression of ADAM9 in neovascular tufts. Representative examples of a neovascular tuft from wild-type (wt) (top) or *Adam9*$^{-/-}$ (9−/−) mice (bottom) stained with anti-ADAM9 (Alexa 488 labeled) (A and B), anti-CD31 (endothelial cell marker, Cy3 labeled in panel A), or anti-NG2 (pericyte marker, Texas Red labeled in panel B) antibody. Merged images are at the right in panels A and B. The expression of ADAM9 in neovascular tufts overlaps that of CD31 but not that of NG2. No staining with ADAM9 antibodies was seen in neovascular tufts that did appear in *Adam9*$^{-/-}$ retinae, confirming that the ADAM9 antibody is specific. (C) Histochemical analysis of sections of tufts stained with anti-ADAM9 or -ADAM15 shows expression of both ADAM9 and ADAM15 in neovascular tufts of wild-type mice but only of ADAM15 in similar sections of *Adam9*$^{-/-}$ mice. (Right) Immunofluorescent analysis of ADAM9 expression in neovascular tufts in retinal sections of a wild-type or *Adam9*$^{-/-}$ mouse. These results confirm that ADAM9 is highly expressed in neovascular tufts.

Reduction of CNV following rupture of Bruch's membrane in *Adam9*$^{-/-}$ mice. CNV originates from choroidal rather than retinal vessels and occurs in completely different disease processes from those in which retinal neovascularization occurs. Unlike retinal neovascularization, ischemia does not appear to be a major stimulus. Adult *Adam9*$^{-/-}$ mice or wild-type controls were subjected to laser photocoagulation (see Materials and Methods for details), mice with rupture of Bruch's membrane were perfused with fluorescein-labeled dextran after 2 weeks, and choroidal flat mounts were examined by fluorescence microscopy. The mean area of CNV at Bruch's membrane rupture sites was significantly smaller in *Adam9*$^{-/-}$ mice ($n = 17$) (a representative image is shown in Fig. 3A) than the mean area of CNV at Bruch's membrane rupture sites in wild-type controls ($n = 20$) (a representative image is shown in Fig. 3B, and a summary of results is shown in Fig. 3C) ($P = 0.0027$).

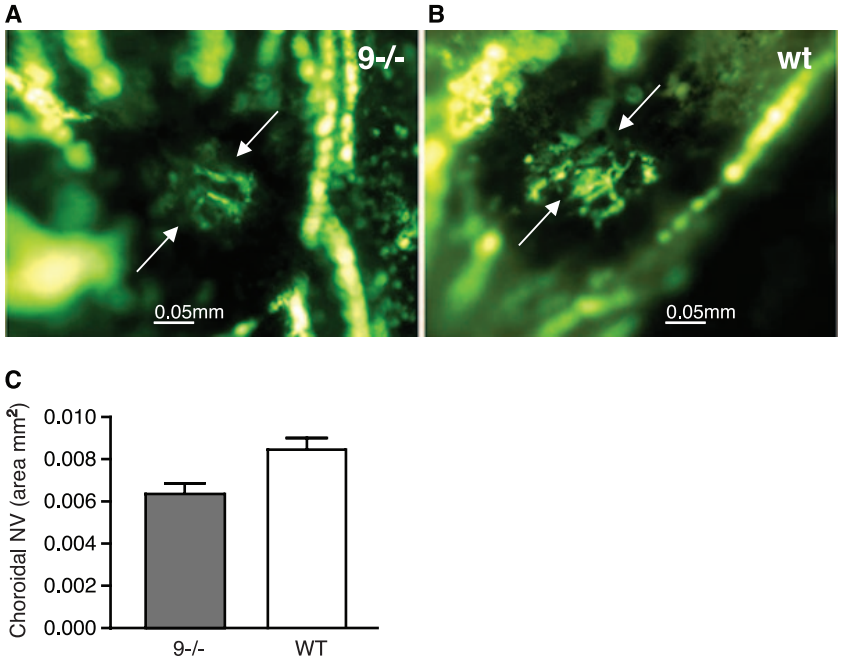

FIG. 3. CNV at Bruch's membrane rupture sites is reduced in *Adam9*$^{-/-}$ mice. After treatment by laser (see Materials and Methods for details), adult *Adam9*$^{-/-}$ mice or wild-type (WT) controls had a rupture of Bruch's membrane in three locations in each eye. After 2 weeks, the mice were perfused with fluorescein-labeled dextran, and choroidal flat mounts were examined by fluorescence microscopy. (A and B) The area of CNV appeared smaller at rupture sites in *Adam9*$^{-/-}$ mice (A) than in wild-type control mice (B). (C) Image analysis confirmed that the area of CNV was significantly smaller in *Adam9*$^{-/-}$ mice than in wild-type mice ($n = 17$ for wild-type mice, and $n = 20$ for *Adam9*$^{-/-}$ mice; $P = 0.0027$).

Reduced growth of heterotopically injected B16F0 melanoma cells in *Adam9*$^{-/-}$ mice. A commonly used approach to evaluate pathological neovascularization is to monitor the growth of heterotopically injected tumor cells in wild-type and knockout mice. To minimize potential effects of the mouse genetic background on this model, we compared tumor growths in litters of wild-type or *Adam9*$^{-/-}$ mice that had been bred from the offspring of a single pair of heterozygous parents (see Materials and Methods for details). In three separate experiments, the average weight of tumors that developed after subcutaneous injection of 1×10^6 B16F0 cells in *Adam9*$^{-/-}$ mice was significantly reduced compared to that of wild-type controls injected with the same culture of cells at the same time (reduction in tumor weight in *Adam9*$^{-/-}$ versus wild-type controls of 54.5%; $n = 29$ [SEM = 0.07] for the wild type versus $n = 29$ [SEM = 0.06] *Adam9*$^{-/-}$ mice; $P < 0.0001$) (Fig. 4A). However, frozen sections of tumors from *Adam9*$^{-/-}$ mice or wild-type controls showed similar sizes and distributions of capillaries as detected by CD31 staining (representative examples are shown in Fig. 4B).

Processing of receptors with roles in angiogenesis by ADAM9 in cell-based assays. The high level of expression of ADAM9 in endothelial cells in retinal vascular tufts of mice subjected to the OIR model as well as the decreased pathological retinal neovascularization and reduced growth of B16F0 tumors in *Adam9*$^{-/-}$ mice raised the possibility that ADAM9 might have important functions in endothelial cells. Since ADAM9 is known to function as a membrane-anchored metalloprotease (10, 15), and because proteolysis can regulate the function of many membrane proteins (1), we hypothesized that ADAM9 could affect pathological neovascularization by

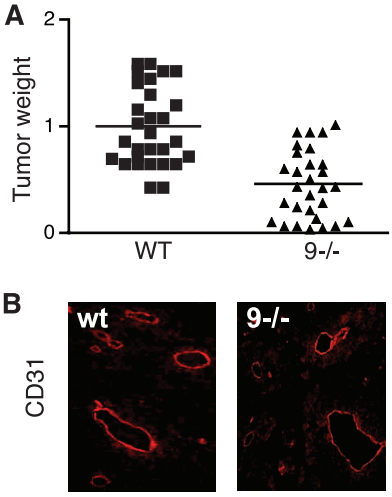

FIG. 4. Growth of heterotopically injected B16F0 melanoma cells in *Adam9*$^{-/-}$ mice and wild-type controls. (A). Relative weights of tumors developing from 10^6 B16F0 melanoma cells injected into the flanks of *Adam9*$^{-/-}$ (9−/−) mice compared to the average of tumor weights in wild-type (WT) control mice that were injected at the same time with the same culture of cells. The data are combined from three separate experiments ($n = 10$ for wild-type mice and $n = 10$ for *Adam9*$^{-/-}$ mice in experiments 1 and 2, and $n = 9$ for wild-type mice and $n = 9$ for *Adam9*$^{-/-}$ mice in experiment 3). Since the tumor sizes in wild-type mice at the end of each experiment varied somewhat, the average tumor size in wild-type mice in each experiment was set to 1, and the tumor size of individual wild-type mice and *Adam9*$^{-/-}$ mice was calculated as a ratio to the average tumor size in wild-type mice. The reduction in tumor size in *Adam9*$^{-/-}$ mice compared to that in wild-type controls was 54.5% ($P < 0.0001$). (B) Representative sections of tumors from wild-type (wt) or *Adam9*$^{-/-}$ mice stained with anti-CD31 to mark endothelial cells. No difference in the overall distribution of larger vessels or capillaries was seen in tumors from wild-type or *Adam9*$^{-/-}$ mice.

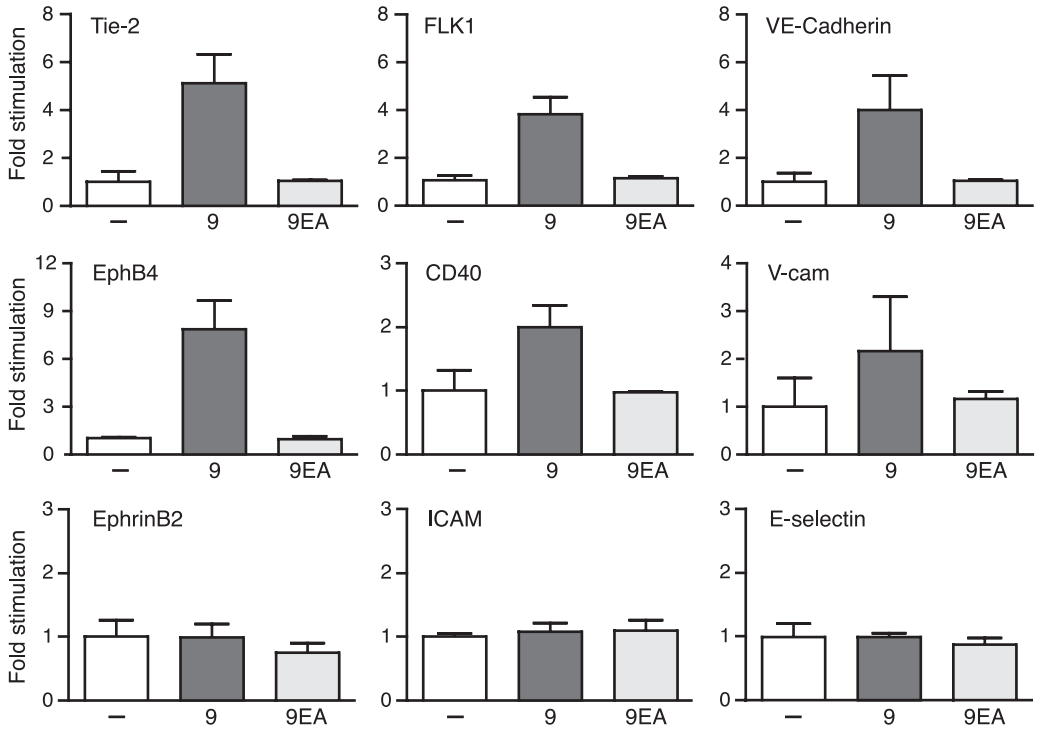

FIG. 5. "Gain-of-function" studies identify substrates for overexpressed ADAM9 with known roles in angiogenesis in cell-based assays. To identify potential substrates of ADAM9 that might be relevant for its function in pathological neovascularization, AP-tagged membrane proteins with known roles in angiogenesis were overexpressed in Cos-7 cells together with empty vector (−), wild-type mouse ADAM9 (9), or the catalytically inactive ADAM9E>A mutant (9EA). The graphs depict the relative AP activity in the supernatant of transfected cells, with the AP activity in cells transfected with a candidate substrate and empty vector set to 1. Each graph is representative of data from at least three separate experiments with two wells per experiment. These results show that overexpressed ADAM9 increases levels of shedding of Tie-2, Flk1 (VEGFR2), VE-cadherin, EphB4, CD40, and VCAM-1 but not of EphrinB2, ICAM, or E-selectin.

processing membrane proteins with roles in angiogenesis and neovascularization. To address this possibility, we overexpressed ADAM9 together with several membrane-anchored receptors with known roles in angiogenesis (CD40, EphrinB2, EphB4, E-selectin, Flk-1, ICAM-1, VCAM-1, Tie-2, VE-cadherin, Flk-1, CD34, and CD36) in Cos-7 cells. Cotransfection of the catalytically inactive ADAM9E>A mutant with candidate substrates served as a control to monitor baseline shedding by endogenous sheddases in Cos-7 cells. Each candidate substrate contained an AP tag in its ectodomain, which facilitated the detection of its shedding into the culture supernatant (17, 29). The overexpression of ADAM9 increased the levels of shedding of Tie-2, Flk-1, VE-cadherin, EphB4, CD40, and VCAM-1 compared to those of the ADAM9E>A control but had no effect on the levels of shedding of EphrinB2, ICAM-1, and E-selectin (Fig. 5) as well as CD34 and CD36 (data not shown). These "gain-of-function" experiments demonstrate that overexpressed ADAM9 enhances the processing of several endothelial cell membrane proteins.

Regulation of ADAM9-dependent shedding by ROS. The ability of overexpressed ADAM9 to cleave substrate proteins in "gain-of-function" experiments raised questions about the role for endogenously expressed ADAM9 in the shedding of these substrates and whether this might be evident in "loss-of-function" experiments in which wild-type cells are compared to *Adam9*$^{-/-}$ cells. To address this question, we treated mEF cells with ROS, which upregulate endogenous ADAM9 in a prostate cancer cell line (22). When mEF cells from wild-type mice were treated with increasing concentrations of H_2O_2 for 6 h, we found a dose-dependent increase in levels of ADAM9 expression (Fig. 6A, bottom). To assess whether this also increased levels of ADAM9-dependent proteolysis, we expressed EphB4, which is efficiently cleaved by overexpressed ADAM9 in Cos-7 cells (see above), in embryonic fibroblasts. Treatment with 50, 100, or 200 μM H_2O_2 for 6 h significantly increased levels of shedding of EphB4 in wild-type mEFs (Fig. 6A, top) but not in *Adam9*$^{-/-}$ cells (Fig. 6B). The increase in levels of ADAM9 expression and EphB4 shedding from wild-type mEFs treated for 6 h with 200 μM H_2O_2 was blocked by actinomycin D, an inhibitor of transcription, which had no effect on the constitutive release of EphB4 (Fig. 6C). The level of shedding of EphB4 from *Adam9*$^{-/-}$ cells could also be increased by transfection with ADAM9; however, this was not further enhanced by ROS (Fig. 6D), presumably because the ADAM9 expression vector lacks the endogenous promoter region with putative ROS response elements. Finally, H_2O_2 treatment of wild-type mEFs did not affect shedding of tumor necrosis factor alpha (TNF-α), a substrate for ADAM17 (Fig. 6E), even though phorbol myristate acetate stimulation of TNF-α shedding, which depends on ADAM17 and not ADAM9 (28), was normal in wild-type cells (Fig. 6F). Taken together, these "loss-of-function" results demonstrate that the upregulation of endogenous ADAM9 via treatment with H_2O_2 results in increased ADAM9-dependent shedding of EphB4.

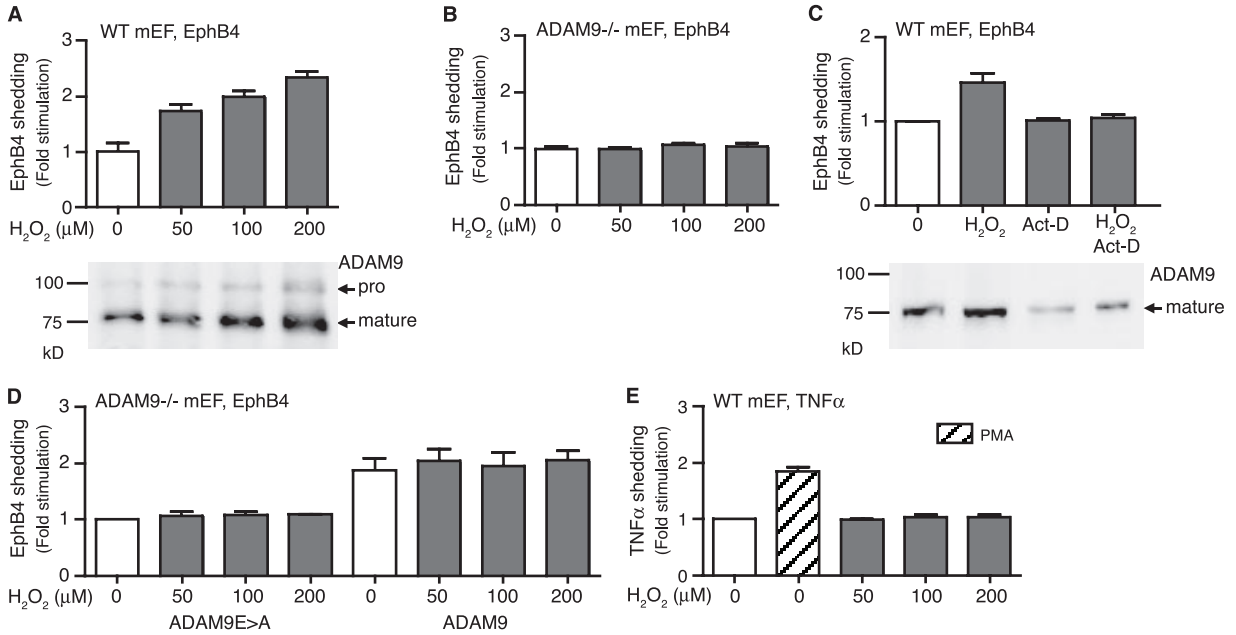

FIG. 6. ROS increase the levels of expression and activity of ADAM9 in mEFs. (A) Wild-type mEFs (50 to 60% culture density) were treated with 50 to 200 μM of H_2O_2 for 6 h, and ADAM9 was detected by Western blotting (bottom). Treatment with H_2O_2 increased the level of expression of ADAM9 in wild-type mEFs. (A and B) Wild-type (A) and *Adam9*$^{-/-}$ (B) mEFs were transfected with EphB4 as a readout for the catalytic activity of endogenous ADAM9 and treated with increasing concentrations of H_2O_2. Increased levels of shedding of EphB4 were seen in an H_2O_2 concentration-dependent manner in wild-type cells (A, top) but not in *Adam9*$^{-/-}$ cells (B), providing the first evidence for processing of a substrate by endogenously upregulated ADAM9 in wild-type cells. (C) Wild-type (WT) mEFs transfected with EphB4 were either not treated or treated with 200 μM H_2O_2, with 1 μg/ml actinomycin D (Act-D), or with both 200 μM H_2O_2 and 1 μg/ml actinomycin D. Actinomycin D prevented the increase in levels of EphB4 shedding from cells treated with H_2O_2 (top) and the increase in ADAM9 protein levels (bottom), suggesting that H_2O_2 enhances the transcription of ADAM9. (D) Levels of shedding of EphB4 from *Adam9*$^{-/-}$ cells can be increased by cotransfection with wild-type ADAM9, but there is no further enhancement by treatment with H_2O_2 (50 to 200 μM). This suggests that ADAM9 is not directly activated by ROS, since the ADAM9 expression plasmid lacks putative ROS transcriptional regulatory elements. (E) Shedding of TNF-α was used to test whether its sheddase, ADAM17, responds to H_2O_2 treatment. Phorbol myristate acetate stimulated the shedding of TNF-α in wild-type mEFs, and this is known to depend on ADAM17 (28), whereas increasing concentrations of ROS did not stimulate the shedding of TNF-α in these cells. These results suggest that ADAM9 is the main sheddase responding to ROS treatment for 6 h in mEF cells.

Since ADAM9 is highly expressed in endothelial cells in pathological neovascular tufts, we examined whether increasing concentrations of H_2O_2 also affected ADAM9 expression and shedding of EphB4 in an immortalized PAE cell line. Western blot analysis confirmed that H_2O_2 also enhanced the levels of ADAM9 in PAE cells compared to untreated cells (Fig. 7A). Moreover, increasing concentrations of H_2O_2 also enhanced the shedding of transfected EphB4 from PAE cells (Fig. 7B). In parallel experiments with PAE cells, we found no effect of increasing concentrations of H_2O_2 on the shedding of the ADAM10 substrate betacellulin (BTC) (Fig. 7C) or the ADAM17 substrate TNF-α (Fig. 7D), neither of which is shed by overexpressed ADAM9 (10, 28). Thus, shedding by ADAM10 or ADAM17 is not measurably activated under the conditions that result in increased levels of expression of ADAM9 and shedding of EphB4 in PAE cells.

DISCUSSION

The mouse model of OIR allows an evaluation of the role of specific molecules in proliferative retinopathies such as retinopathy of prematurity (4, 8, 21). In the OIR model, relative hypoxia following the exposure of mice to high concentrations of oxygen (75%) and return to room air (21% oxygen) stimulates the production of hypoxia-inducible factor 1 and then VEGF in order to attract new vessels (4, 21). This results in the proliferation of vascular cells in the retina and the formation of pathological vascular tufts, potentially leading to temporary or permanent blindness. The current study provides the first evidence for an important role of ADAM9 in ischemia-induced retinal neovascularization. CNV occurs in diseases with abnormalities in the retinal pigmented epithelium and Bruch's membrane, such as age-related macular degeneration. CNV is modeled by rupturing Bruch's membrane with laser photocoagulation in mice, and ADAM9 was also a contributor in this model. In addition to its function in these two types of ocular neovascularization, ADAM9 is also required for the growth of heterotopically injected melanoma cells in mice.

The strong decrease in levels of ocular neovascularization in *Adam9*$^{-/-}$ mice compared to wild-type controls demonstrates that ADAM9 has a role in the development of pathological vessels in the retina and choroid. On the other hand, we found no significant difference in developmental retinal angiogenesis between *Adam9*$^{-/-}$ mice and age-matched wild-type controls at P6. This is consistent with the high level of expression of ADAM9 in pathological neovascular tufts that develop in mice subjected to the OIR model but that are not present during

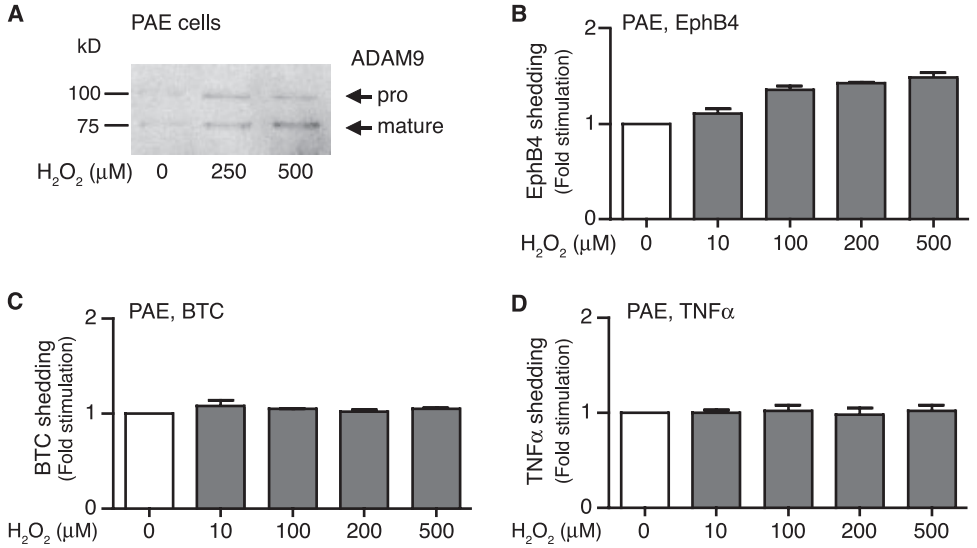

FIG. 7. Treatment of PAE cells with ROS enhances expression of ADAM9 and shedding of EphB4. (A) The level of expression of ADAM9 in immortalized PAE cells was increased by treatment with 250 or 500 μM H_2O_2. Expression of ADAM9 was detected by Western blotting with antibodies against the cytoplasmic domain of human ADAM9. (B to D) Increasing concentrations of H_2O_2 (10 to 500 μM) enhanced the shedding of transfected EphB4 from PAE cells (B) but had no effect on the shedding of the ADAM10 substrate BTC (C) or the ADAM17 substrate TNF-α (D). Since EphB4 can be cleaved by overexpressed ADAM9, whereas BTC and TNF-α are not (10, 28), these results suggest that H_2O_2 stimulates ADAM9-dependent shedding of EphB4 in PAE cells.

normal development of the retinal vasculature. Within the neovascular tufts, ADAM9 appears to be expressed in endothelial cells, as it colocalized with the endothelial cell marker CD31 but not with the pericyte marker NG2. Interestingly, cells positive for the pericyte marker NG2 and cells expressing ADAM9 or CD31 are closely intermingled in neovascular tufts, suggesting that the interactions between endothelial cells and pericytes are altered in these structures compared to normal vessels and capillaries, where pericytes are usually found ensheathing and surrounding endothelial cells.

Immediately after exposure to high oxygen in the OIR model, whole mounts of retinae from both *Adam9*$^{-/-}$ mice and wild-type controls displayed central avascular areas of approximately similar size (data not shown), so the vascular regression caused by high oxygen levels was not detectably affected in the absence of ADAM9. In wild-type mice subjected to the OIR model, revascularization of the retinal bed occurred over 5 days after return to normoxia, whereas this process was strongly delayed in *Adam9*$^{-/-}$ mice, even 8 days after return to room air (data not shown). Thus, ADAM9 appears to have an important role in the generation of new capillaries that grow into the central avascular area following vascular regression. Moreover, the reduction in CNV in *Adam9*$^{-/-}$ mice suggests that ADAM9, similarly to the related protein ADAM15 (26), also contributes to the development of new vessels triggered by stimuli other than ischemia. Finally, the significantly reduced growth of B16F0 melanoma cells in *Adam9*$^{-/-}$ mice compared to that of wild-type controls is consistent with a role for ADAM9 in the formation of the tumor vasculature, although ADAM9 could also be involved in other host-derived contributions to tumor growth, such as the release of growth factors from fibroblasts or macrophages. The observation that tumor sections from *Adam9*$^{-/-}$ and wild-type mice showed no differences in the sizes and distribution patterns of blood vessels suggests that tumor growth in *Adam9*$^{-/-}$ mice could have been delayed by the ability of the vasculature to keep up with tumor growth, which would nevertheless require an even distribution of vessels and capillaries in the absence of ADAM9.

Since ADAM9 is a membrane-anchored metalloprotease, which has been implicated in the processing of membrane proteins such as EGF or FGFR2iiib (10, 15), we hypothesized that dysregulated ADAM9 could perhaps process membrane proteins on the surface of endothelial cells, thereby ultimately promoting pathological neovascularization. We found that overexpressing ADAM9 increased the shedding of CD40, EphB4, Flk-1, Tie-2, VE-cadherin, and VCAM compared to the inactive ADAM9E>A control, raising the possibility that dysregulated ADAM9 also increases the processing of these molecules in endothelial cells in vivo. Since overexpressed ADAM9 can shed the majority of the candidate substrates tested here, it is likely that it can also release additional membrane proteins from endothelial cells besides the ones assessed here. Therefore, dysregulated ADAM9 could have a significant impact on the turnover and processing of endothelial cell surface molecules. Since very little is currently known about how ectodomain shedding affects the function of individual endothelial cell surface proteins, it is possible that the role of ADAM9 in pathological neovascularization depends on the processing of one functionally dominant cell surface protein or on the sum of the consequences of processing several different types of cell surface proteins on endothelial cells. Further studies aimed at understanding how shedding affects the function of individual endothelial cell membrane proteins will be necessary to address this question. In addition, other noncatalytic protein modules of ADAM9, such as its disintegrin domain, cysteine-rich region, or cytoplasmic domain, could be important for the function of ADAM9 in neovascularization.

The contribution of the catalytic activity of ADAM9 compared to that of its other protein domains can be assessed, for example, by generating a knock-in point mutation in the catalytic site of ADAM9 in mice that will inactivate its catalytic activity without affecting its other protein domains.

With respect to the upregulation of ADAM9 in neovascular tufts, it is interesting that studies of prostate cancer cells have shown a strong enhancement of ADAM9 expression after treatment with ROS such as H_2O_2. Since ROS are also thought to contribute to proliferative retinopathy (9, 27), we tested whether H_2O_2 could increase the expression of endogenous ADAM9 in wild-type mEF cells and, more importantly, whether this would also affect ADAM9-dependent ectodomain shedding. We chose EphB4 (one of the candidate substrates found to be released upon ADAM9 overexpression in Cos-7 cells) as a representative model substrate to assess the activation of ADAM9-dependent ectodomain shedding by ROS. Although ADAM9 was not required for the shedding of EphB4 from unstimulated mEF cells (a separate study will be focused on identifying the constitutive sheddase for EphB4) (our unpublished data), we observed a time- and H_2O_2 dose-dependent increase in levels of shedding of EphB4 from wild-type cells but not from *Adam9*$^{-/-}$ cells. This correlated with increased ADAM9 protein levels in wild-type mEF cells treated with H_2O_2. These results suggest that the upregulation of endogenous ADAM9 changes the relative contribution of this ADAM protein to the shedding of EphB4 such that ADAM9 becomes a major sheddase for EphB4 in cells treated with H_2O_2 but not in untreated cells.

When *Adam9*$^{-/-}$ cells expressing EphB4 were rescued by transfection with ADAM9, there was a substantial increase in the level of EphB4 shedding, but this was not further enhanced by H_2O_2 treatment. Evidently, the effect of ROS on the activity of ADAM9 is not posttranslational, such as by promoting the removal of its inhibitory prodomain. Instead, since the plasmid used to overexpress ADAM9 in *Adam9*$^{-/-}$ mEFs lacks the transcriptional regulatory elements of endogenous ADAM9, and since ROS-stimulated shedding by endogenous ADAM9 in wild-type cells could be blocked by inhibiting transcription with actinomycin D, the regulation of endogenous ADAM9 by ROS most likely occurs at the transcriptional level. Additional evidence that ROS specifically enhances ADAM9-dependent shedding and not shedding by ADAM17 came from experiments with the ADAM17 substrate TNF-α, whose release from mEF cells was not activated by ROS. Moreover, the expression of ADAM9 and shedding of EphB4 could also be stimulated in a pig aortic endothelial cell line by increasing concentrations of ROS, whereas shedding of TNF-α or of the ADAM10 substrate BTC was not. Taken together, these results provide the first evidence, to our knowledge, that ROS not only upregulate the expression of ADAM9 but also increase levels of ADAM9-dependent ectodomain shedding in cell-based assays.

Based on these results, it is tempting to speculate that ROS are also responsible, at least in part, for the high level of expression of ADAM9 in retinal neovascular tufts in mice subjected to the OIR model. Sudden changes in tissue oxygenation increase the imbalance between free radicals and antioxidants, and larger amounts of ROS are normally produced under hypoxic conditions, especially in tissues with a high metabolic rate such as the retina. This could affect many signaling pathways, including the activation of ADAM9 expression, particularly at the junction of the vascular and avascular retina, where the difference in tissue oxygen levels is likely greatest, and in premature infants who might have a reduced ability to scavenge reactive oxidative species (9, 27). Since little is currently know about the transcriptional regulation of ADAM9, it will now be interesting to learn more about how ROS, hyperoxia, or relative hypoxia regulates the expression of this gene.

In summary, the response of *Adam9*$^{-/-}$ mice in models of retinal neovascularization and CNV and a heterotopic tumor model suggests that ADAM9 has a critical role in pathological neovascularization. Since ADAM9 can process several membrane proteins that are expressed on endothelial cells, it is tempting to speculate that an increase in the level of processing of these and other endothelial cell membrane proteins is the primary stimulus for pathological retinal neovascularization in these models, although noncatalytic functions of ADAM9 could also be involved in this process. Importantly, this study is the first to demonstrate that ADAM9-dependent ectodomain shedding can be enhanced by the treatment of cells with ROS as a consequence of the increased level of expression of ADAM9. Taken together, these results suggest that ADAM9 might be a good target for the treatment of pathological neovascularization, which has a critical role in the pathogenesis of a variety of diseases including proliferative retinopathies, age-related macular degeneration, rheumatoid arthritis, and cancer.

ACKNOWLEDGMENTS

This work was supported by National Institutes of Health grants from the Eye Institute to C.P.B. (grant EY15759) and to P.C. (grant EY12609).

We thank Viktoriya Nikolenko and Joshua Namm for excellent technical assistance and Shahin Rafii for providing access to his confocal microscope.

REFERENCES

1. **Blobel, C. P.** 2005. ADAMs: key players in EGFR-signaling, development and disease. Nat. Rev. Mol. Cell Biol. **6:**32–43.
2. **Blobel, C. P., D. G. Myles, P. Primakoff, and J. W. White.** 1990. Proteolytic processing of a protein involved in sperm-egg fusion correlates with acquisition of fertilization competence. J. Cell Biol. **111:**69–78.
3. **Bradley, J., M. Ju, and G. S. Robinson.** 2007. Combination therapy for the treatment of ocular neovascularization. Angiogenesis **10:**141–148.
4. **Chen, J., and L. E. Smith.** 2007. Retinopathy of prematurity. Angiogenesis **10:**133–140.
5. **Folkman, J., and D. Ingber.** 1992. Inhibition of angiogenesis. Semin. Cancer Biol. **3:**89–96.
6. **Friedlander, M., M. I. Dorrell, M. R. Ritter, V. Marchetti, S. K. Moreno, M. El-Kalay, A. C. Bird, E. Banin, and E. Aguilar.** 2007. Progenitor cells and retinal angiogenesis. Angiogenesis **10:**89–101.
7. **Fruttiger, M.** 2007. Development of the retinal vasculature. Angiogenesis **10:**77–88.
8. **Hammes, H. P., M. Brownlee, A. Jonczyk, A. Sutter, and K. T. Preissner.** 1996. Subcutaneous injection of a cyclic peptide antagonist of vitronectin receptor-type integrins inhibits retinal neovascularization. Nat. Med. **2:**529–533.
9. **Hardy, P., I. Dumont, M. Bhattacharya, X. Hou, P. Lachapelle, D. R. Varma, and S. Chemtob.** 2000. Oxidants, nitric oxide and prostanoids in the developing ocular vasculature: a basis for ischemic retinopathy. Cardiovasc. Res. **47:**489–509.
10. **Horiuchi, K., S. Le Gall, M. Schulte, T. Yamaguchi, K. Reiss, G. Murphy, Y. Toyama, D. Hartmann, P. Saftig, and C. Blobel.** 2007. Substrate selectivity of EGF-receptor ligand sheddases and their regulation by phorbol esters and calcium influx. Mol. Biol. Cell **18:**176–188.
11. **Horiuchi, K., G. Weskamp, L. Lum, H. P. Hammes, H. Cai, T. A. Brodie, T. Ludwig, R. Chiusaroli, R. Baron, K. T. Preissner, K. Manova, and C. P. Blobel.** 2003. Potential role for ADAM15 in pathological neovascularization in mice. Mol. Cell. Biol. **23:**5614–5624.

12. **Khong, T. L., H. Larsen, Y. Raatz, and E. Paleolog.** 2007. Angiogenesis as a therapeutic target in arthritis: learning the lessons of the colorectal cancer experience. Angiogenesis **10:**243–258.
13. **Nath, D., P. M. Slocombe, A. Webster, P. E. Stephens, A. J. Docherty, and G. Murphy.** 2000. Meltrin gamma (ADAM-9) mediates cellular adhesion through alpha(6)beta(1)integrin, leading to a marked induction of fibroblast cell motility. J. Cell Sci. **113:**2319–2328.
14. **Olsson, A. K., A. Dimberg, J. Kreuger, and L. Claesson-Welsh.** 2006. VEGF receptor signalling—in control of vascular function. Nat. Rev. Mol. Cell Biol. **7:**359–371.
15. **Peduto, L., V. E. Reuter, D. R. Shaffer, H. I. Scher, and C. P. Blobel.** 2005. Critical function for ADAM9 in mouse prostate cancer. Cancer Res. **65:** 9312–9319.
16. **Roghani, M., J. D. Becherer, M. L. Moss, R. E. Atherton, H. Erdjument-Bromage, J. Arribas, R. K. Blackburn, G. Weskamp, P. Tempst, and C. P. Blobel.** 1999. Metalloprotease-disintegrin MDC9: intracellular maturation and catalytic activity. J. Biol. Chem. **274:**3531–3540.
17. **Sahin, U., G. Weskamp, Y. Zheng, V. Chesneau, K. Horiuchi, and C. P. Blobel.** 2006. A sensitive method to monitor ectodomain shedding of ligands of the epidermal growth factor receptor. Methods Mol. Biol. **327:**99–113.
18. **Sahin, U., G. Weskamp, H. M. Zhou, S. Higashiyama, J. J. Peschon, D. Hartmann, P. Saftig, and C. P. Blobel.** 2004. Distinct roles for ADAM10 and ADAM17 in ectodomain shedding of six EGFR-ligands. J. Cell Biol. **164:** 769–779.
19. **Sherris, D.** 2007. Ocular drug development—future directions. Angiogenesis **10:**71–76.
20. **Shigemura, K., S. Y. Sung, H. Kubo, R. S. Arnold, M. Fujisawa, A. Gotoh, H. E. Zhau, and L. W. Chung.** 2007. Reactive oxygen species mediate androgen receptor- and serum starvation-elicited downstream signaling of ADAM9 expression in human prostate cancer cells. Prostate **67:**722–731.
21. **Smith, L. E., E. Wesolowski, A. McLellan, S. K. Kostyk, R. D'Amato, R. Sullivan, and P. A. D'Amore.** 1994. Oxygen-induced retinopathy in the mouse. Investig. Ophthalmol. Vis. Sci. **35:**101–111.
22. **Sung, S. Y., H. Kubo, K. Shigemura, R. S. Arnold, S. Logani, R. Wang, H. Konaka, M. Nakagawa, S. Mousses, M. Amin, C. Anderson, P. Johnstone, J. A. Petros, F. F. Marshall, H. E. Zhau, and L. W. Chung.** 2006. Oxidative stress induces ADAM9 protein expression in human prostate cancer cells. Cancer Res. **66:**9519–9526.
23. **Tobe, T., S. Ortega, J. D. Luna, H. Ozaki, N. Okamoto, N. L. Derevjanik, S. A. Vinores, C. Basilico, and P. A. Campochiaro.** 1998. Targeted disruption of the FGF2 gene does not prevent choroidal neovascularization in a murine model. Am. J. Pathol. **153:**1641–1646.
24. **Weskamp, G., H. Cai, T. A. Brodie, S. Higashyama, K. Manova, T. Ludwig, and C. P. Blobel.** 2002. Mice lacking the metalloprotease-disintegrin MDC9 (ADAM9) have no evident major abnormalities during development or adult life. Mol. Cell. Biol. **22:**1537–1544.
25. **Weskamp, G., J. R. Krätzschmar, M. Reid, and C. P. Blobel.** 1996. MDC9, a widely expressed cellular disintegrin containing cytoplasmic SH3 ligand domains. J. Cell Biol. **132:**717–726.
26. **Xie, B., J. Shen, A. Dong, M. Swaim, S. F. Hackett, L. Wyder, S. Worpenberg, S. Barbieri, and P. A. Campochiaro.** 2008. An Adam15 amplification loop promotes vascular endothelial growth factor-induced ocular neovascularization. FASEB J. **22:**2775–2783.
27. **Yeh, P. T., C. M. Yang, J. S. Huang, C. T. Chien, C. H. Yang, Y. H. Chiang, and Y. F. Shih.** 2008. Vitreous levels of reactive oxygen species in proliferative diabetic retinopathy. Ophthalmology **115:**734–737.
28. **Zheng, Y., P. Saftig, D. Hartmann, and C. Blobel.** 2004. Evaluation of the contribution of different ADAMs to TNFα shedding and of the function of the TNFα ectodomain in ensuring selective stimulated shedding by the TNFα convertase (TACE/ADAM17). J. Biol. Chem. **279:**42898–42906.
29. **Zheng, Y., J. Schlondorff, and C. P. Blobel.** 2002. Evidence for regulation of the tumor necrosis factor alpha-convertase (TACE) by protein-tyrosine phosphatase PTPH1. J. Biol. Chem. **277:**42463–42470.
30. **Zigrino, P., J. Steiger, J. W. Fox, S. Loffek, A. Schild, R. Nischt, and C. Mauch.** 2007. Role of ADAM-9 disintegrin-cysteine-rich domains in human keratinocyte migration. J. Biol. Chem. **282:**30785–30793.